Laser induced zero-group velocity resonances in transversely isotropic cylinder

Jérôme Laurent[a)] and Daniel Royer

ESPCI ParisTech, PSL Research University, CNRS, Institut Langevin, 1 rue Jussieu, F-75005 Paris, France

Takasar Hussain and Faiz Ahmad

School of Natural Sciences, National University of Sciences and Technology, Sector H-12, Islamabad, Pakistan

Claire Prada

ESPCI ParisTech, PSL Research University, CNRS, Institut Langevin, 1 rue Jussieu, F-75005 Paris, France

The transient response of an elastic cylinder to a laser impact is studied. When the laser source is a line perpendicular to the cylinder axis, modes guided along the cylinder are generated. For a millimetric steel cylinder up to ten narrow resonances can be locally detected by a laser interferometer below 8 MHz. These resonances correspond to Zero-Group Velocity guided modes or to circumferential modes. The authors observe that the theory describing the propagation of elastic waves in an isotropic cylinder is not sufficient to precisely predict the resonance spectrum. In fact, the texture of such elongated structure manifests as elastic anisotropy. Thus, a transverse isotropic (TI) model is used to calculate the dispersion curves and compare them with the measured ones, obtained by moving the source along the cylinder. The five elastic constants of a TI cylinder are adjusted, leading to a good agreement between measured and theoretical dispersion curves. Then, all the resonance frequencies are satisfactorily identified. © 2015 Acoustical Society of America.
[http://dx.doi.org/10.1121/1.4921608]

I. INTRODUCTION

Elongated cylindrical structures like rods, cable strands, or fibers are widely used in the industry or in civil engineering. Characterization of mechanical properties of constitutive materials is important for testing their structural integrity. Non-Destructive Evaluation (NDE) of these properties is usually carried out with elastic waves. Various methods like Resonant Ultrasonic Spectroscopy/pulse-echo contact-method, or pulsed/continuous Laser-Ultrasound (LU) contactless-method are used. Cylindrical structures support the propagation along their axes of elastic waves of different types: longitudinal (L), flexural (F), or torsional (T). Many theoretical and numerical studies and few experimental results were published the past 50 years on the propagation of time harmonic guided modes in solid or hollow cylinders.[1–3] In the 19th century, Pochhammer[4] and Chree[5] first established the equation of longitudinal waves in free isotropic cylindrical structures. In 1943, Hudson studied the fundamental flexural mode in a solid cylinder[6] and longitudinal modes of a bar were examined by Davies[7] in 1948. Gazis reported the first exact solutions of the frequency equation,[1] as well as a complete description of propagative modes, displacement, and stress distributions for an isotropic elastic hollow cylinder in vacuum. Pao and Mindlin[8,9] as well as Onoe *et al.*[10] studied all the branches of the complete three-dimensional problem of a free solid cylinder. A thorough review of elastic wave propagation in isotropic elastic cylinders and plates was given by Meeker and Meitzler.[3] Later, Zemanek investigated elastic wave propagation in a cylinder, both experimentally and theoretically.[11]

All these works deal with isotropic material, however transverse anisotropy is exhibited by elongated cylindrical structures due to their manufacturing processes (poly-crystalline metals)[12] or their texture (carbon fibers used in reinforced polymers). Then, non-destructive measurement of elastic constants of transverse isotropic (TI) materials is of great interest,[13] especially in aeronautic and aerospace industries. Morse first established the frequency equation for longitudinal waves propagating in TI cylinders.[14] The extension of Gazis formulation to orthotropic and TI waveguides was initiated by Mirsky in 1964 for infinite and finite cylinders.[15,16] Then, several researchers investigated the propagation or the scattering of elastic waves in free or fluid-loaded TI cylinders.[17–21] Ahmad and Rahman[22] also studied the scattering of acoustic wave incident on a TI cylinder and showed that Buchwald's representation[23] yields much simpler equations.[24] This representation is beneficial to simplify the description of the potential functions and economizes laborious calculations. This model provides perfectly similar results with the models of Honarvar and Sinclair[25] and Honarvar *et al.*[26] and can be applied to study both isotropic and TI cylinders. Honarvar *et al.* also obtained the frequency equations of axisymmetric and asymmetric free vibrations of finite TI cylinders.[27] Several other researchers proposed to use the impedance matrix theory[28,29] or a semi-analytical finite element method to study transient thermoelastic waves in isotropic/anisotropic cylinders.[30]

Frequency equations determining the angular frequency $\omega(=2\pi f)$ versus the axial wave number $k(=2\pi/\lambda)$ have to be solved numerically. For a given circumferential order n, the various solutions (integer m) can be grouped into different families: longitudinal L(0, m) and torsional T(0, m) modes with displacements independent of the azimuthal angle θ, or flexural

---

a)Electronic mail: jerome.laurent@espci.fr

F(n, m) modes with displacements varying as sin $n\theta$ or cos $n\theta$. Each mode is represented by a dispersion curve $\omega(k)$. Many similarities exist between the families of modes found in plates and cylinders. Indeed, torsional modes T(0, m) are similar to shear horizontal modes SH in plates. Longitudinal L(0, m) and first flexural F(1, m) modes in cylinders are analogous to symmetrical S_m and anti-symmetrical A_m Lamb modes in plates. Major differences appear in the frequency spectrum for flexural modes F(n, m) with family number $n \geq 2$.

The laser-based ultrasonic technique is a convenient tool for the generation and detection of guided elastic waves in plates[31] or cylinders.[32] It has been shown that this non-contact technique is very efficient to observe Zero Group Velocity (ZGV) Lamb modes corresponding to a frequency minimum of the dispersion curves $\omega(k)$.[33,34] At the ZGV frequencies, guided modes have a finite phase velocity but vanishing group velocity. The interference of forward and backward guided waves having opposite wave numbers gives rise to a standing wave pattern.[35] For these specific points, the energy deposited by the laser pulse remains trapped under the source. The resulting local and narrow resonances can be detected at the epicenter with an optical interferometer. This non-contact method allowed us to perform accurate measurements of elastic properties of isotropic or TI materials.[36,37] For cylinders, a line laser source can be used to control the propagation direction. For a line source parallel to the cylinder axis, circumferential Rayleigh and whispering gallery waves are excited, giving rise to resonances at all n integer values of the normalized circumferential wave number[38] ka. This configuration was also used by Mounier *et al.* to study resonances of a micrometric fiber at sub-gigahertz frequencies and to determine the elastic constants using an isotropic model.[39] Circumferential resonances occur at cutoff frequencies of longitudinal and flexural modes where the axial wave number vanishes. They are analogous to thickness resonances in plates at cutoff frequencies of Lamb modes. In the case of a TI cylinder, this configuration is not appropriate to determine the whole set of elastic constants.

In this paper, we investigate the mechanical response of a transversely isotropic cylinder to a laser line source perpendicular to the axis. In this case, the generated waves guided along the cylinder axis are sensitive to the material anisotropy. We performed measurements in a millimeter steel cylinder and many resonances are observed in the megahertz range. They can be roughly identified from the minimum frequency of some branches of the dispersion curves of longitudinal and flexural modes calculated for an isotropic cylinder. However, significant discrepancies remain between the isotropic model and experimental resonance frequencies. Dispersion curves are then calculated using a TI model. The five independent elastic constants are adjusted such that all measured resonance frequencies can be precisely predicted. Moreover, experimental dispersion curves, measured by moving the laser source, are compared with the theoretical ones.

II. EXPERIMENTS

Measurements were performed with an optical interferometer at the center of the source. Compared to a point source, the use of a laser line perpendicular to the cylinder axis significantly reduces the excitation of most circumferential modes. Resonances were extracted from the spectrum of the temporal signal. Their frequencies were compared with minimum frequencies of dispersion curves calculated from an isotropic material.

A. Laser-ultrasonic setup

The experimental setup is shown Fig. 1. The sample is an austenitic stainless steel (AISI 304L, Weber Metaux, Paris) solid cylinder (length 420 mm, diameter $2a = 0.775$ mm, and mass density is $\rho = 7.91 \times 10^3 \, \text{kg m}^{-3}$). The rod is supported by two beveled metallic pieces to reduce the mechanical contact (friction). Elastic waves were generated by a Q-switched Nd:YAG (yttrium aluminum garnet) laser providing 8-ns pulses of 15-mJ energy at a 100-Hz repetition rate (Quantel Centurion). The spot diameter of the unfocused beam is equal to 2.5 mm. A beam expander ($\times 4$) and a cylindrical lens (focal length 250 mm) were used to enlarge and focus the laser beam into a narrow line on the surface. The optical energy distribution was close to a Gaussian and the absorbed power density was below the ablation threshold. The full length of the source at $1/e$ of the maximum value was found to be 10 mm and the width was estimated to be 0.3 mm. In the thermoelastic regime, the line source is equivalent to a set of force dipoles distributed on the surface and parallel to the cylinder axis.[40] The estimated Rayleigh range of the Gaussian laser beam (0.8 mm) is only twice the cylinder radius (0.39 mm). Then, the energy deposited along the cylinder circumference depends on the azimuthal angle θ. Moreover, the optical absorption decreases with θ from the normal incidence ($\theta = 0$) on both sides of the sample. *A priori*, this asymmetry favors the excitation of some flexural modes.

Local vibrations were measured by a heterodyne interferometer equipped with a 100-mW frequency doubled Nd:YAG laser (optical wavelength $\Lambda = 532$ nm). This interferometer is sensitive to any phase shift $\Delta\phi$ along the path of the optical probe beam, and then to the mechanical displacement u_r normal to the surface. The calibration factor (85 nm/V), deduced from the phase modulation $\Delta\phi = 2\pi u_r/\Lambda$ of the reflected beam, was constant over the detection bandwidth (20 kHz–20 MHz). Large low frequency phase-shifts due to
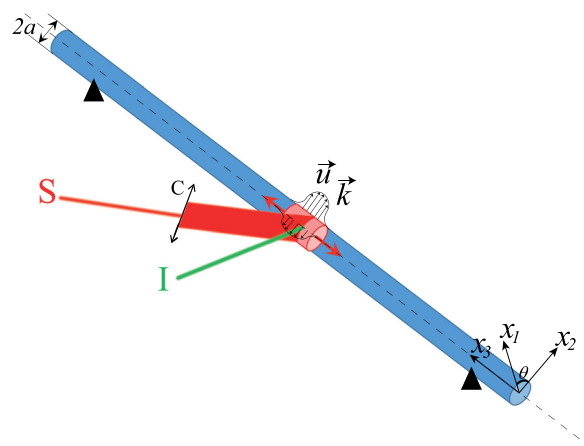

FIG. 1. (Color online) Source and probe geometry used to excite and to detect local resonances in a cylinder. *S*: laser source, *I*: interferometer, *C*: cylindrical lens.

thermal effect or first flexural F(1,1) mode are eliminated by interposing, before amplification, a high-pass filter having a cutoff frequency equal to 1.5 MHz.[41] Measurements were conducted at room temperature (21 ± 0.5 °C). Signals detected by the optical probe were fed into a digital sampling oscilloscope and transferred to a computer.

B. Zero-group velocity resonances

The propagation of elastic waves along the cylinder axis is represented by dispersion curves calculated from Zemanek's equation.[11] The steel sample is assumed to be homogeneous with longitudinal and transverse velocities $V_L = 5650$ m/s and $V_T = 3010$ m/s, respectively. The numerical algorithm used to find the roots of the secular equation was proposed by Seco and Jiménez.[42] First, the cutoff frequencies are evaluated with a bisection method, then a zero-finding algorithm is applied to determine each branch successively. The roots were obtained with an acceptable error of less than 10^{-6}. Finally, the dispersion curves are determined for longitudinal modes and the first seven families of flexural modes in less than 1 min on a personal computer, with a resolution $\Delta k = 10^{-3}$ mm^{-1}. As shown in Fig. 2(a), dispersion curves obtained for longitudinal L(0, m) and first flexural F(1, m) modes are similar to those obtained for an isotropic elastic plate. Dispersion curves of higher order flexural modes F(n, m) are plotted in Fig. 2(b). As the interferometer is only sensitive to the normal displacement, torsional modes are not presented. Branches of the dispersion curves are obtained separately, thus ZGV frequencies are easily determined by searching for minimum frequencies for finite wave numbers.

A typical signal, corresponding to the mechanical displacement normal to the cylinder surface, is given in Fig. 3(a). As previously explained, the oscillations in the first 5 μs are due to the large displacements associated with the low frequency components of the flexural mode F(1, 1) similar to the A_0 mode in plates. As shown in the insert, the low amplitude tail for $t > 5$ μs is not noise but high frequency oscillations due to ZGV or circumferential resonances. The spectra of out-off plane displacement are shown in Fig. 3(b). Seven resonances dominate between 1.5 and 8 MHz. The peak at 2.77 MHz can be ascribed to the ZGV resonance at the minimum frequency of the F(2, 1)-mode, while peaks at 4.38 and 4.29 MHz correspond to L(0, 2) and F(3, 1)-ZGV modes, respectively. The peak at 3.42 MHz can be associated with a circumferential resonance [horizontal arrow in Fig. 2(a)] at the cutoff frequency (3.46 MHz) of the F(1, 3) mode. The peak at 5.61 MHz is relatively close to the minimum frequency (5.79 MHz) of the F(4, 1) mode. Higher frequency peaks at 6.83 and 7.70 MHz do not correspond to any minimum frequency on the dispersion curves. Except for L(0,2) which is estimated at 0.2%, relative errors from 2% to 4% are observed for the other resonances. The good agreement for the L(0, 2) and F(1, 3) resonances was obtained with the chosen pair of bulk wave velocities. Another pair of velocities ($V_L = 5500$ m/s, $V_T = 2920$ m/s) is needed to accurately predict the resonance frequencies of higher order modes ($n \geq 2$). Thus, the isotropic model with two elastic constants is not suitable. A higher number of material parameters are required for a better prediction of the resonance frequencies. In Sec. III, we apply the model with five elastic constants, developed by Ahmad and Rahman for TI cylinder.[22]

The Q-factor ($Q = f_0/\Delta f_0$) can be estimated from the half-power width Δf_0 of the resonance peak at the ZGV
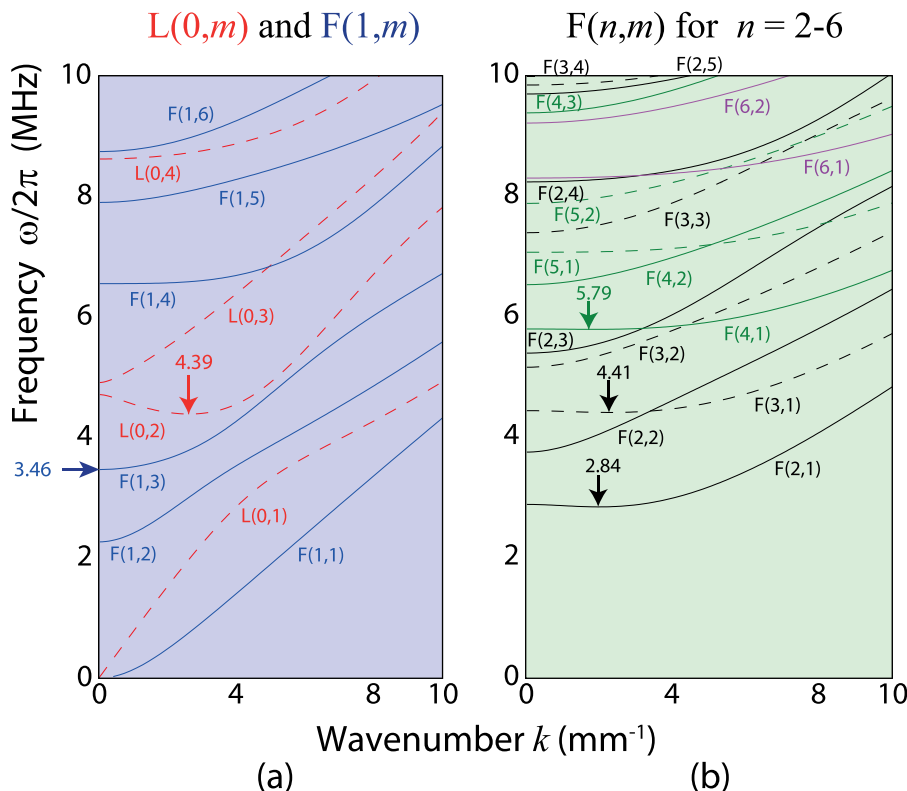

FIG. 2. (Color online) Dispersion curves for an isotropic stainless steel solid cylinder (diameter 0.775 mm). (a) Longitudinal L(0, m) and first flexural F(1, m) modes. (b) Higher order flexural modes F(n, m). Vertical arrows indicate minimum frequencies corresponding to ZGV modes.

J. Acoust. Soc. Am., Vol. 137, No. 6, June 2015

Laurent et al.: Resonances in transversely isotropic cylinder   3327
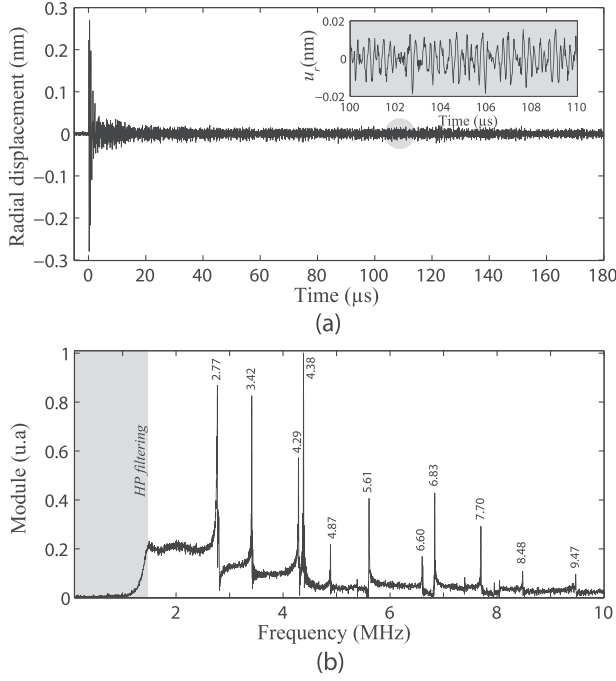
FIG. 3. (a) Radial displacement measured by the optical interferometer. Inset: zoom on a portion of the temporal displacement. (b) Frequency spectrum filtered by an analog high-pass filter ($f \leq 1.5$ MHz).

point. In order not to underestimate the Q-factor, the signal acquisition time window Θ must be larger than the inverse of the bandwidth. We performed a measurement of the out-of-plane displacement at the epicenter with a signal acquisition time window $\Theta = 4$ ms. We obtained thinnest resonances and a Q-factor at L(0, 2)-ZGV frequency of 4×10^3 ($\Delta f = 1.1$ kHz and $f_0 = 4.38$ MHz). For flexural ZGV resonances, the Q-factors are slightly lower and vary from 2×10^3 to 2.5×10^3. With such high Q values, the influence of the ultrasound attenuation can be neglected.

III. TI MODEL

In the linear theory of elasticity, anisotropic media are described by the stiffness tensor c_{ijkl} (with $i, j, k, l = 1$–3). Using the Voigt's notation, they are represented by a 6×6 symmetric matrix $c_{\alpha\beta}$ ($\alpha, \beta = 1$–6). Given the Cartesian coordinates (x_1, x_2, x_3) with the x_3-axis parallel to the cylinder z axis, the sample is supposed to be isotropic in the (x_1, x_2) plane. Such TI medium is described by five independent elastic constants: c_{11}, c_{13}, c_{33}, c_{44}, and c_{66}. Other elastic constants are related to these coefficients: $c_{22} = c_{11}$, $c_{23} = c_{13}$, $c_{55} = c_{44}$, $c_{12} = c_{11} - 2c_{66}$ or vanish.

A. Dispersion equation

As mentioned by Honarvar et al.,[26] the displacement vector $\boldsymbol{u}(r, \theta, z, t)$ can be derived from three scalar potential functions φ, χ, and ψ.[25,43] A simple representation initiated by Buchwald[23] and used by Ahmad and Rahman[22] is the following:

$$\boldsymbol{u} = \nabla\varphi + \nabla \times (\chi\hat{e}_z) + \left(\frac{\partial\psi}{\partial z} - \frac{\partial\varphi}{\partial z}\right)\hat{e}_z. \quad (1)$$

In cylindrical coordinates (r, θ, z), the above representation leads to the following displacement components:

$$(u_r, u_\theta, u_z) = \left(\frac{\partial\varphi}{\partial r} + \frac{1}{r}\frac{\partial\chi}{\partial\theta}, \frac{1}{r}\frac{\partial\varphi}{\partial\theta} - \frac{\partial\chi}{\partial r}, \frac{\partial\psi}{\partial z}\right).$$

Harmonic solutions are given by

$$\varphi_n = \Phi J_n(\beta r) \cos(n\theta) \exp[i(kz - \omega t)],$$
$$\psi_n = \Psi J_n(\beta r) \cos(n\theta) \exp[i(kz - \omega t)],$$
$$\chi_n = X J_n(\beta r) \sin(n\theta) \exp[i(kz - \omega t)],$$

where J_n is the Bessel function of the first kind of order n. They correspond to the superposition of plane waves of wave vector $\boldsymbol{k} = (\beta \cos \theta, \beta \sin \theta, k)$ which satisfy the propagation equation in a meridian plane. The radial component β of the wave vector $\boldsymbol{k}$ must satisfy the *Christoffel* equation

$$(c_{11}c_{44}\beta^4 - E\beta^2 + F)(c_{66}\beta^2 + c_{44}k^2 - \rho\omega^2) = 0. \quad (2)$$

The first term corresponds to waves polarized in the meridian plane (x_2, x_3) and the second term corresponds to pure shear wave (polarized along x_1). The coefficients E and F are given in the Appendix [Eq. (A2)]. The above equations are similar to those obtained by Mirsky.[16] Omitting the propagation term $\exp i(kz - \omega t)$ for simplicity, the three independent solutions are found to be

$$(\varphi_{1n}, \psi_{1n}, \chi_{1n}) = (J_n(\beta_1 r)\cos(n\theta), q_1 J_n(\beta_1 r)\cos(n\theta), 0),$$
$$(\varphi_{2n}, \psi_{2n}, \chi_{2n}) = (q_2 J_n(\beta_2 r)\cos(n\theta), J_n(\beta_2 r)\cos(n\theta), 0),$$
$$(\varphi_{3n}, \psi_{3n}, \chi_{3n}) = (0, 0, J_n(\beta_3 r)\sin(n\theta)).$$

The three roots of the *Christoffel* equation, β_1, β_2, and β_3 are given in Eq. (A3) and q_1, q_2 are the potential amplitude ratios provided by Eq. (A4). Hence, the displacements are as follows:

$$(u_{1r}, u_{1\theta}, u_{1z})_n = \left(\beta_1 J_n'(\beta_1 r)\cos(n\theta), -\left(\frac{n}{r}\right)J_n(\beta_1 r)\sin(n\theta), ikq_1 J_n(\beta_1 r)\cos(n\theta)\right),$$
$$(u_{2r}, u_{2\theta}, u_{2z})_n = \left(q_2\beta_2 J_n'(\beta_2 r)\cos(n\theta), -\left(\frac{n}{r}\right)q_2 J_n(\beta_2 r)\sin(n\theta), ik J_n(\beta_2 r)\cos(n\theta)\right),$$
$$(u_{3r}, u_{3\theta}, u_{3z})_n = \left(\left(\frac{n}{r}\right)J_n(\beta_3 r)\cos(n\theta), -\beta_3 J_n'(\beta_3 r)\sin(n\theta), 0\right). \quad (3)$$

Laurent et al.: Resonances in transversely isotropic cylinder

The first two solutions correspond to a coupling between quasi-longitudinal and quasi-shear waves polarized in the meridian plane. The last solution having zero displacement component along the z axis corresponds to a pure shear wave. These solutions must be combined with weighting factors B_n, C_n, D_n to satisfy the boundary conditions at the free surface $r = a$. These conditions imply that normal stresses vanish: $\sigma_{rr}(a) = \sigma_{r\theta}(a) = \sigma_{rz}(a) = 0$ and lead to the following homogeneous linear system:

$$\begin{bmatrix} a_{11} & a_{12} & a_{13} \\ a_{21} & a_{22} & a_{23} \\ a_{31} & a_{32} & a_{33} \end{bmatrix} \begin{bmatrix} B_n \\ C_n \\ D_n \end{bmatrix} = \begin{bmatrix} 0 \\ 0 \\ 0 \end{bmatrix}, \tag{4}$$

where the matrix elements a_{ij} are listed in Eq. (A1). The dispersion equation results from the secular equation

$$\det(a_{ij}) = 0. \tag{5}$$

For $n = 0$, Eq. (5) splits into two parts: $a_{23} = 0$, i.e., $(\beta_3 a)J_0''(\beta_3 a) = J_0'(\beta_3 a)$ similar to the equation given by Mirsky[16] for torsional modes $T(0, m)$ and $a_{11}a_{32} = a_{12}a_{31}$ corresponding to longitudinal modes $L(0, m)$.

B. Cutoff frequencies

As the wave number k is equal to zero, the motion at the cutoff frequencies is independent of the axial coordinate x_3. This implies $k^2 q_1 = 0$, $q_2 = 0$, and $a_{12} = a_{22} = 0$. The dispersion equation [Eq. (5)] for longitudinal and flexural modes in a solid cylinder at $k = 0$ reduces to

$$\beta_2 a J_n'(\beta_2 a)(a_{13}a_{21} - a_{11}a_{23}) = 0, \tag{6}$$

where the four a_{ij} simplify as

$$a_{11} = c_{11}(\beta_1 a)^2 J_n''(\beta_1 a) + c_{12}\{(\beta_1 a)J_n'(\beta_1 a) - n^2 J_n(\beta_1 a)\},$$
$$a_{13} = 2nc_{66}\{(\beta_3 a)J_n'(\beta_3 a) - J_n(\beta_3 a)\},$$
$$a_{21} = -2n\{(\beta_1 a)J_n'(\beta_1 a) - J_n(\beta_1 a)\},$$
$$a_{23} = -(\beta_3 a)^2 J_n''(\beta_3 a) + (\beta_3 a)J_n'(\beta_3 a) - n^2 J_n(\beta_3 a).$$

To find the cutoff frequencies, the above equation can be solved for $\omega_c (= 2\pi f_c)$, for various values of n and m. The first two roots $\beta_{1,2}$ are simplified using the reduced expressions of $\Delta = (c_{11} - c_{44})\rho\omega_c^2$, $E = (c_{11} - c_{44})\rho\omega_c^2$, and $F = \rho^2\omega_c^4$ [Eq. (A3)] as $\beta_1 = \omega_c\sqrt{\rho/c_{11}}$ and $\beta_2 = \omega_c\sqrt{\rho/c_{44}}$. The third root reduces to $\beta_3 = \omega_c\sqrt{\rho/c_{66}}$. The cutoff frequency equation [Eq. (6)] is simplified as $a_{11}J_n'(\beta_2 a) = 0$ for $L(0, m)$.

C. Dependence of ZGV frequencies on elastic constants

A sensitivity analysis was performed to characterize the elastic constant influence on the dispersion curves and especially on ZGV frequencies. Figure 4 displayed the longitudinal and the first two flexural mode families as a function of elastic constants.

Each constant was successively varied by $\pm 5\%$ and $\pm 10\%$ around the following average values (in GPa):

$c_{11} = 240$, $c_{13} = 110$, $c_{33} = 250$, $c_{44} = 70$, and $c_{66} = 70$. The curves obtained for the average values are displayed by the dashed line. It appears that each ZGV resonance depends on specific constants. For example, the elastic constants which mainly affect the $L(0, 2)$-ZGV frequency are c_{11} and c_{44}. These elastic constants are proportional to the square of longitudinal and shear velocities in directions perpendicular to the cylinder axis x_3. While $F(1, 4)$-ZGV frequency slightly depends on c_{11} and more strongly on c_{44} and c_{66} which is proportional to the square of the shear velocity in the direction perpendicular to the cylinder axis. When the values of c_{11}, c_{13}, and c_{33} increase or when c_{44}, c_{66} decrease, the $F(1, 4)$-ZGV frequency disappears, i.e., the slope of the spectral line at the cutoff frequency becomes positive. It should be noted that $F(2, 1)$-ZGV frequency is almost independent of the first four elastic constants while it significantly depends on c_{66}.

IV. RESULTS AND DISCUSSION

In this section, we identify all the resonance frequencies and accurately determine the five elastic constants. The experimental dispersion curves were fitted with those obtained theoretically with the TI model.[22] Then, we compared isotropic and TI models to highlight the anisotropy of the stainless steel cylinder.

A. Dispersion curves measurements

Experimental dispersion curves were measured with the laser ultrasound setup displayed in Fig. 1. The out-of-plane displacement was recorded with the interferometer at a single point in the middle of the cylinder, while the line source was moved on 40 mm along the cylinder axis by 0.1 mm steps. For each source position, the normal displacement was recorded during 180 μs at a 50 MHz sampling frequency. To increase the signal to noise ratio, 1024 signals were averaged. First, apodization (Hanning) windows were applied in both dimensions (time and distance) to avoid secondary lobes. Then, a two-dimensional Fourier transform was applied to the obtained B-scans. Since cylindrical waveguides support backward-propagation with opposite group and phase velocities,[35] the spatial Fourier transform was extended to negative wave numbers [Fig. 5(b)].

The counter propagative modes are observed in the cylinder both for longitudinal and flexural modes and occur in the vicinity of $k = 0$. For example, at the $L(0, 2)$-ZGV frequency (4.34 MHz) the $L(0, 2)$ and $L(0, 3)b$ modes having opposite wave vectors interfere. The power spectrum was computed at a frequency of 4.40 MHz, slightly higher than the $L(0, 2)$-ZGV resonance frequency, for which the modes are propagative. Figure 5(a) shows that this spectrum is composed of two main peaks. The peak at a negative value of k, similar to the larger one in the positive k domain, demonstrates the backward propagation in cylinders. Afterwards, the dispersion curves (backward region) for negative wave number $\omega(-k)$ were folded and added to positive ones [Fig. 5(c)]. We can clearly identify five ZGV frequencies. One at 4.34 MHz corresponding to the $L(0, 2)$-ZGV resonance and four others at 2.77, 4.28, 5.60, and 6.60 MHz corresponding to $F(2, 1)$, $F(3, 1)$, $F(4, 1)$, and $F(1, 4)$ flexural-ZGV resonances,
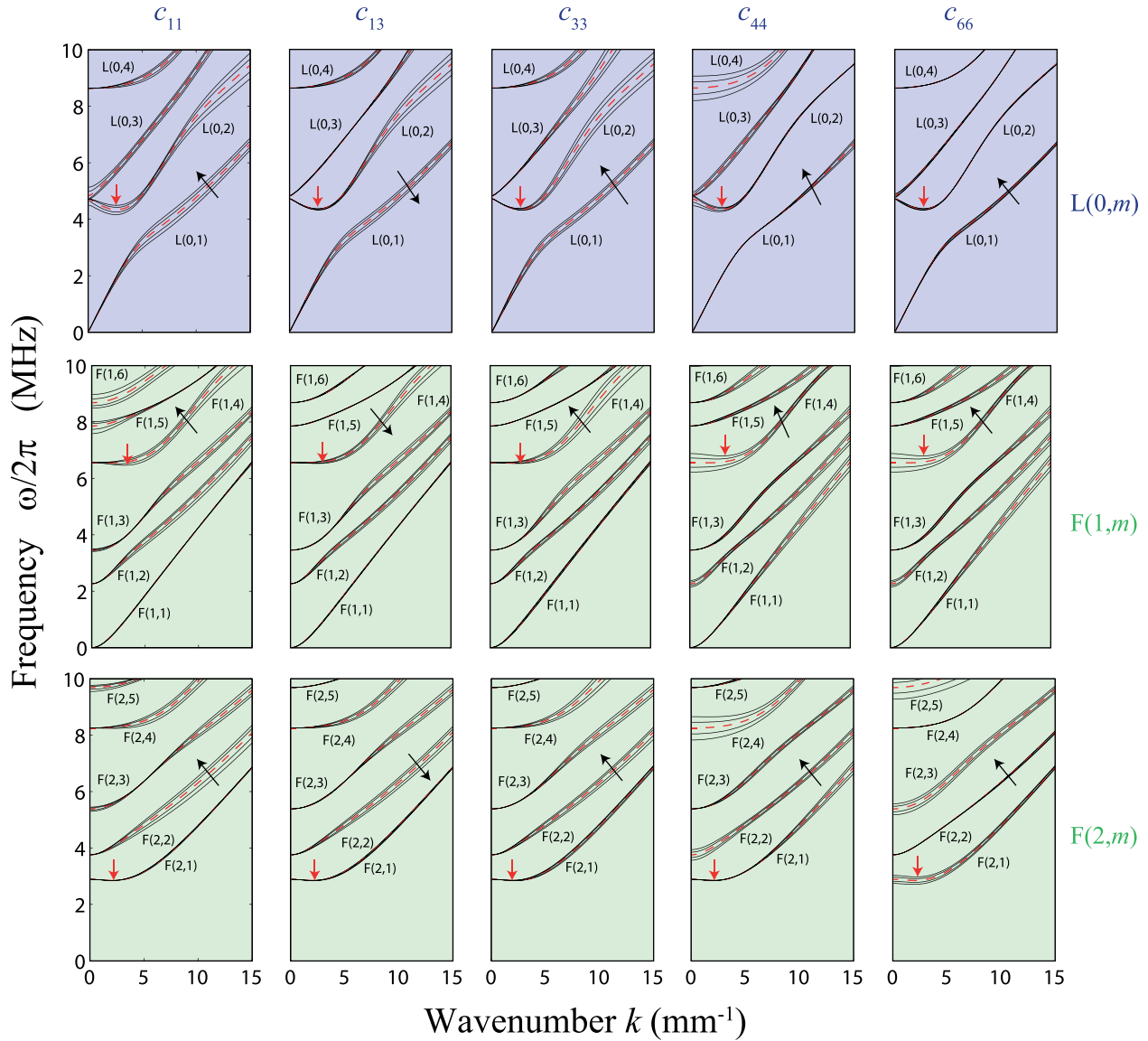
FIG. 4. (Color online) Influence of the elastic constants on the dispersion curves of a transversely isotropic cylinder. From top to bottom: for longitudinal modes and the first two flexural mode families. Vertical arrows depict the ZGV frequencies and tilted arrows show increasing c_{ij}.

respectively. The wavelengths at these ZGV frequencies extend from 2.3 to 3.2 mm ($\lambda/2a \sim 3$–4) except for F(1, 4)-ZGV frequency which has a 14.3 mm wavelength ($\lambda/2a \sim 18.6$).

The theoretical dispersion relation $\omega(k)$ [Eq. (5)] was calculated by solving the secular equation with the zero-finding algorithm.[42] Experimental dispersion curves were fitted with the TI model. Bulk modes whose bulk velocities are proportional to stiffness constants c_{33} and c_{44} were eliminated by dividing the determinant by $(\rho\omega^2 - c_{33}k^2)(\rho\omega^2 - c_{44}k^2)$. We calculated longitudinal modes and the first seven families of flexural modes. Starting from the two pairs of bulk wave velocities previously determined with the isotropic model, theoretical dispersion curves were fitted heuristically (i.e., without any minimization algorithm) by adjusting the five elastic constants. Finally, we observe [Fig. 5(c)] good agreement between experimental dispersion curves and those predicted by the TI model. The parameters used for the TI model are listed in Table I. The dashed and

dotted lines correspond to the longitudinal and first flexural modes, respectively, the solid and long-dashed lines indicated the flexural modes with $n \geq 2$. Although most modes are well fitted by the theory, a few experimental branches are not explained. This may be due to a small remaining error on the estimated constants or to a slight discrepancy with transverse anisotropy.

B. Elastic parameters

We now explain the physical meaning of the five sound velocities implicitly involved in the TI model. Stiffness constants c_{11} and c_{33} determine the longitudinal (L) ultrasound velocities in perpendicular (V_{L1}) and parallel (V_{L3}) directions with respect to the cylinder axis x_3,

$$c_{11} = \rho V_{L1}^2, \quad c_{33} = \rho V_{L3}^2. \tag{7}$$

Stiffness constants c_{44} and $c_{66} = (c_{11} - c_{12})/2$ determine the shear (S) velocities in directions perpendicular to the
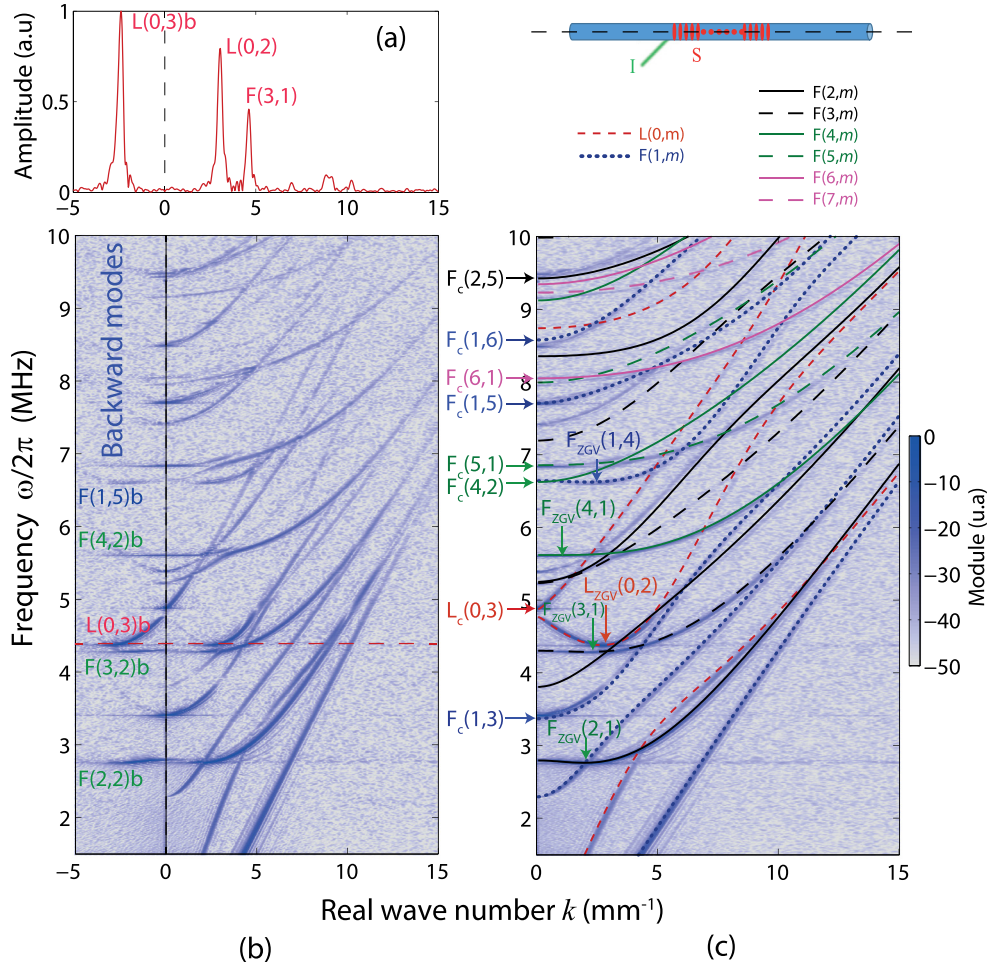
FIG. 5. (Color online) (a) Spatial Fourier transform of the normal displacement at 4.40 MHz illustrating backward propagation with a negative wave number. Each backward mode is coupled to the upper mode of the same family $(n, m+1)$. To avoid confusion they are indicated by the index b. (b) Experimental dispersion curves obtained for negative and positive wave numbers. (c) Negative dispersion curves $\omega(-k)$ were folded and added to the positive ones. The experimental dispersion curves were fitted with the TI model (the control parameters used are listed in Table I).

cylinder axis with polarizations either perpendicular (V_{S1}) or parallel (V_{S3}) to the x_3-axis

$$c_{44} = \rho V_{S1}^2, \quad c_{66} = \rho V_{S3}^2. \tag{8}$$

The remaining stiffness constant c_{13} should be adjusted manually. Hence, two Young's modulus can be defined: $E_\parallel = E_{33}$ for a stress parallel to the cylinder axis and $E_\perp = E_{11} = E_{22}$ for a stress perpendicular to the cylinder axis. They are given by

$$E_\parallel = \frac{c^2}{c_{11} - c_{66}}, \quad E_\perp = \frac{4 c_{66} c^2}{c^2 + c_{33} c_{66}}, \tag{9}$$

where $c^2 = c_{33}(c_{11} - c_{66}) - c_{13}^2$ is the determinant of the sub-matrix of elastic constants c_{ij}. This effective stiffness constant c is proportional to the bar velocity of the waves propagating along the cylinder axis: $V_b = (E_\parallel/\rho)^{1/2}$ [see Eq. (44) of Mirsky[16]]. Three Poisson's ratios[44,45] can be defined, ν_{12} and ν_{31} for longitudinal extension in the basal plane and ν_{13} along the six-fold axis

$$\nu_{12} = \frac{c_{12} c_{33} - c_{13}^2}{c^2 + c_{33} c_{66}}, \quad \nu_{31} = \frac{2 c_{66} c_{13}}{c^2 + c_{33} c_{66}}, \quad \nu_{13} = \frac{c_{13}}{c_{11} + c_{12}}.$$

C. Comparison between isotropic and TI model

Theoretical dispersion curves obtained with isotropic (dashed lines) and transversely isotropic (solid lines) models are plotted in Fig. 6. The longitudinal modes are displayed in Fig. 6(a) and the first six flexural mode families [Figs. 6(b)–6(g)]. The frequency spectrum recorded at the epicenter is shown in Fig. 6(h). This representation allows to distinguish the different propagation modes and to precisely identify each resonance peak. It obviously appears that the isotropic model
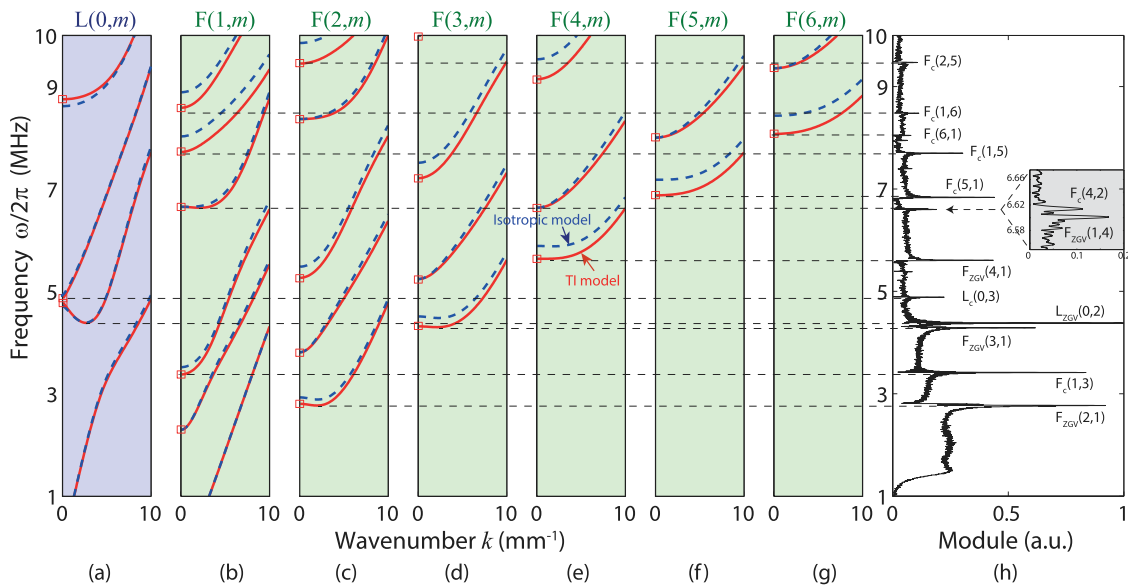
TABLE I. Elastic constants c_{ij} (or sound velocities) used in the TI model. a and ρ were measured.

Stiffness constants (GPa)					
c_{11}	c_{12}	c_{13}	c_{33}	c_{44}	c_{66}
239	109	110	252	72	65
Sound velocities (m/s)					Diameter (μm)
V_{L1}	V_{S1}	V_{L3}	V_{S3}	V_b	2a
5500	2875	5650	3010	4808	775 $\pm$ 2
Young's modulus (GPa)		Poisson's ratio			Density (kg/m³)
$E_\perp$	$E_\parallel$	ν_{12}	ν_{13}	ν_{31}	ρ
183	172	0.317	0.316	0.298	7910 $\pm$ 5

FIG. 6. (Color online) Comparison of isotropic model (dashed lines) with TI model (solid lines). (a) Longitudinal modes L(0, m). (b)–(g) Flexural modes F(n, m) for n extends from 1 to 6. (h) Frequency spectrum recorded at epicenter. The subscript c denotes the cutoff frequencies. Inset: two resonance frequencies are observed corresponding to F(1, 4)-ZGV and F_c(4, 2), respectively. The squares indicate the cutoff frequencies calculated with Eq. (6).

is not appropriate to interpret experimental results and clearly confirms the TI nature of the cylinder. Five ZGV resonances, F(2, 1), F(3, 1), L(0, 2), F(4, 1), F(1, 4), and eight circumferential resonances, F(1, 3), L(0, 3), F(4, 2), F(5, 1), F(1, 5), F(6, 1), F(1, 6), and F(2, 5), can be identified from the dispersion curves calculated with the TI model. Both ZGV and cutoff frequencies are estimated with a relative error less than 0.6%, except for F_c(1, 3) for which the error is close to 1.1%.

D. Displacements at cutoff frequencies

In order to explain why several circumferential resonances (at $k = 0$) are observed while others are not, we analyzed the displacements generated inside the cylinder. To this end,

we calculated u_r, u_θ, and u_z, using Eq. (3). The radial and axial displacements (u_r) and (u_z) were calculated at $\theta = 0$ and the azimuthal displacement (u_θ) at $\theta_{max} = \pi/2n$. They are displayed in Fig. 7 at the cutoff frequencies of the modes L(0, 3), L(0, 4), F(1, 2), and F(1, 3) which, respectively, correspond to the frequencies 4.834, 8.673, 2.276, and 3.343 MHz. For L_c(0, 3) and F_c(1, 3) circumferential resonances, the radial displacement at the cylinder surface $r = a$ is significant. Conversely, for the modes L_c(0, 4) and F_c(1, 2) the radial displacement vanishes for $r = a$, but have essentially a large displacement along the z axis. This explains why, at these cutoff frequencies, no resonances are observed.

V. CONCLUSION

In summary, elastic guided waves propagating in a stainless steel cylinder of millimetric diameter were investigated by laser ultrasonic techniques. Using a laser line source perpendicular to the cylinder axis, ZGV resonances were observed both for longitudinal and flexural modes. One of the major interests is to identify each resonance to characterize elastic properties of materials. We demonstrated that isotropic model was not relevant to describe the behaviour of elastic guided waves in a steel rod. A TI model allowed us to describe the propagation and to calculate dispersion curves $\omega(k)$. The five elastic constants were estimated from experimental dispersion curves measured by the LU technique. A good agreement between theoretical and experimental dispersion curves was obtained both for longitudinal and flexural modes.

In the future, it would be useful to build a numerical inversion procedure to improve the accuracy of the material parameter estimation. Furthermore, it will be interesting to investigate the relationship between ZGV modes and elastic constants. This could be done by calculating the second order derivatives of the dispersion curves at cutoff frequencies to determine the existence of backward modes. Finally, it will be interesting to conduct other studies in materials with different types of
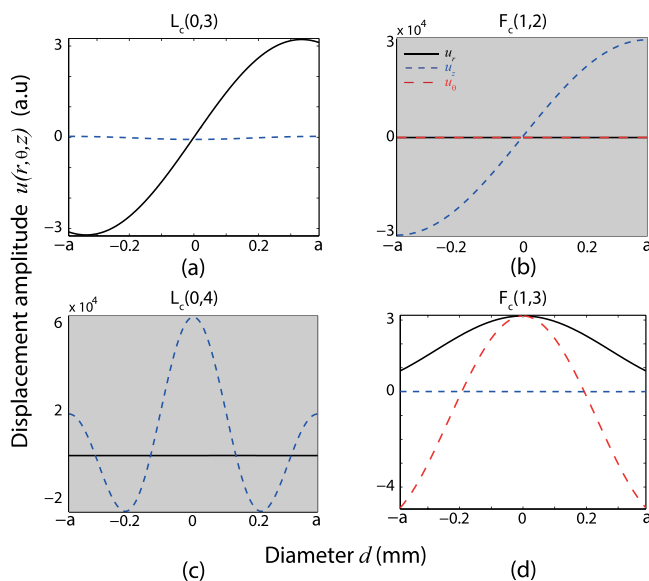

FIG. 7. (Color online) Displacement components produced at (a) L(0, 3), (b) F(1, 2), (c) L(0, 4), and (d) F(1, 3) cutoff frequencies. The solid, dashed, and long-dashed lines indicate u_r, u_θ, and u_z, respectively.

anisotropy. This technique can be also applied in the sub-gigahertz range with a laser line source of width comparable to the cylinder diameter to study micrometric fibers.

APPENDIX

The scalar functions φ, χ, and ψ satisfy the following wave motion equations:

$$c_{11}\left(\mathbf{V}^2 - \frac{\partial^2}{\partial z^2}\right)\varphi + c_{44}\frac{\partial^2 \varphi}{\partial z^2} + (c_{13} + c_{44})\frac{\partial^2 \psi}{\partial z^2} = \rho\frac{\partial^2 \varphi}{\partial t^2},$$

$$(c_{13} + c_{44})\left(\mathbf{V}^2 - \frac{\partial^2}{\partial z^2}\right)\varphi + c_{44}\left(\mathbf{V}^2 - \frac{\partial^2}{\partial z^2}\right)\psi$$
$$+ c_{33}\frac{\partial^2 \psi}{\partial z^2} = \rho\frac{\partial^2 \psi}{\partial t^2},$$

$$c_{66}\left(\mathbf{V}^2 - \frac{\partial^2}{\partial z^2}\right)\chi + c_{44}\frac{\partial^2 \chi}{\partial z^2} = \rho\frac{\partial^2 \chi}{\partial t^2}.$$

The longitudinal L (represented by φ) and the vertically polarized quasi-transverse SV (represented by ψ) waves are coupled, whereas the pure transverse wave SH (represented by χ) is decoupled from the others. The dispersion equation of torsional, longitudinal, and flexural guided modes in a transversely isotropic cylinder with free boundary conditions results in the vanishing of the determinant of a 3×3 matrix a_{ij},

$$\det(a_{ij}) = \begin{cases} a_{23} = 0 & \text{for } T(0,m), \\ a_{11}a_{32} - a_{12}a_{31} = 0 & \text{for } L(0,m), \\ a_{11}(a_{22}a_{33} - a_{23}a_{32}) - \\ a_{12}(a_{21}a_{33} - a_{23}a_{31}) + \\ a_{13}(a_{21}a_{32} - a_{22}a_{31}) = 0 & \text{for } F(n \geq 1, m), \end{cases}$$

where the matrix elements are

$$a_{11} = c_{11}(\beta_1 a)^2 J_n''(\beta_1 a)$$
$$+ c_{12}\{(\beta_1 a)^2 J_n'(\beta_1 a) - n^2 J_n(\beta_1 a)\}$$
$$- c_{13}q_1(ka)^2 J_n(\beta_1 a),$$

$$a_{12} = c_{11}q_2(\beta_2 a)^2 J_n''(\beta_2 a)$$
$$+ c_{12}q_2\{(\beta_2 a)J_n'(\beta_2 a) - n^2 J_n(\beta_2 a)\}$$
$$- c_{13}(ka)^2 J_n(\beta_2 a),$$

$$a_{13} = 2nc_{66}\{(\beta_3 a)J_n'(\beta_3 a) - J_n(\beta_3 a)\},$$

$$a_{21} = -2n\{(\beta_1 a)J_n'(\beta_1 a) - J_n(\beta_1 a)\},$$

$$a_{22} = -2nq_2\{(\beta_2 a)J_n'(\beta_2 a) - J_n(\beta_2 a)\},$$

$$a_{23} = -(\beta_3 a)^2 J_n''(\beta_3 a) + (\beta_3 a)J_n'(\beta_3 a) - n^2 J_n(\beta_3 a),$$

$$a_{31} = (1 + q_1)(\beta_1 a)J_n'(\beta_1 a),$$

$$a_{32} = (1 + q_2)(\beta_2 a)J_n'(\beta_2 a),$$

$$a_{33} = nJ_n(\beta_3 a), \tag{A1}$$

respectively. The first and second derivatives of the Bessel function of the first kind of order n can be expressed in terms of J_{n-1}, J_n, J_{n+1}, etc., by using recurrence relations. The coefficients E and F used in the *Christoffel* equation [Eq. (2)] are defined as

$$E = (c_{13} + c_{44})^2 k^2 + c_{44}(\rho\omega^2 - c_{44}k^2) + c_{11}(\rho\omega^2 - c_{33}k^2)$$
$$= E_1^2 + c_{44}F_1 + c_{11}F_2,$$
$$F = (\rho\omega^2 - c_{44}k^2)(\rho\omega^2 - c_{33}k^2) = F_1 F_2. \tag{A2}$$

Finally, the three roots (β) of the *Christoffel* equation are

$$\beta_{1,2} = \sqrt{\frac{E \mp \Delta}{2c_{11}c_{44}}} \quad \text{and} \quad \beta_3 = \sqrt{\frac{F_1}{c_{66}}}, \tag{A3}$$

where $\Delta = \sqrt{E^2 - 4c_{11}c_{44}F}$. At last, the amplitude ratio q_1 and q_2 are given by

$$q_1 = \frac{F_1 - c_{11}\beta_1^2}{kE_1}, \quad q_2 = \frac{kE_1}{F_1 - c_{11}\beta_2^2}. \tag{A4}$$

[1]D. C. Gazis, "Three-dimensional investigation of the propagation of waves in hollow circular cylinders. Part I. Analytical foundation," J. Acoust. Soc. Am. **31**, 568–573 (1959); "Three-dimensional investigation of the propagation of waves in hollow circular cylinders. Part II. Numerical results," *ibid.* **31**, 573–578 (1959).

[2]R. Mindlin and H. McNiven, "Axially symmetric waves in elastic rods," J. Appl. Mech. **27**, 145–151 (1960).

[3]T. Meeker and A. Meitzler, "Guided wave propagation in elongated cylinders and plates," Phys. Acoust. **1**, 111–167 (1964).

[4]L. Pochhammer, "Über die fortplanzungsgeschwindigkeiten kleiner schwingungen in einem unbegrenzten isotropen kreiscylinder" ("On the propagation velocities of small vibrations in an infinite isotropic circular cylinder"), J. Reine Angew. Math. **81**, 324–336 (1876).

[5]C. Chree, "The equations of an isotropic elastic solid in polar and cylindrical coordinates, their solution and applications," Trans. Cambridge Philos. Soc. **14**, 250–369 (1889).

[6]G. E. Hudson, "Dispersion of elastic waves in solid circular cylinders," Phys. Rev. **63**, 46–50 (1943).

[7]R. Davies, "A critical study of the Hopkinson pressure bar," Philos. Trans. R. Soc. **240**, 375–457 (1948).

[8]Y.-H. Pao and R. Mindlin, "Dispersion of flexural waves in an elastic, circular cylinder," J. Appl. Mech. **27**, 513–520 (1960).

[9]Y.-H. Pao, "The dispersion of flexural waves in an elastic circular cylinder, Part 2," J. Appl. Mech. **29**, 61–64 (1962).

[10]M. Onoe, H. McNiven, and R. Mindlin, "Dispersion of axially symmetric waves in elastic rods," J. Appl. Mech. **29**, 729–734 (1962).

[11]J. Zemanek, Jr., "An experimental and theoretical investigation of elastic wave propagation in a cylinder," J. Acoust. Soc. Am. **51**, 265–283 (1972).

[12]T. Mason, "Variation in the dispersion of axisymmetric waves in infinite circular rods with crystallographic wire texture," J. Acoust. Soc. Am. **106**, 1262–1270 (1999).

[13]R. G. Payton, *Elastic Wave Propagation in Transversely Isotropic Media*, Vol. 4 (Martinus Nijhoff Publishers, The Hague, 1983).

[14]R. Morse, "Compressional waves along an anisotropic circular cylinder having hexagonal symmetry," J. Acoust. Soc. Am. **26**, 1018–1021 (1954).

[15]I. Mirsky, "Axisymmetry vibrations of orthotropic cylinders," J. Acoust. Soc. Am. **36**, 2106–2112 (1964).

[16]I. Mirsky, "Wave propagation in transversely isotropic circular cylinders, Part I: Theory," J. Acoust. Soc. Am. **37**, 1016–1021 (1965); "Wave propagation in transversely isotropic circular cylinders, Part II: Numberical results," *ibid.* **37**, 1022–1026 (1965).

[17]F. C. Eliot and G. Mott, "Elastic waves propagation in circular cylinders having hexagonal crystal symmetry," J. Acoust. Soc. Am. **44**, 423–430 (1968).

J. Acoust. Soc. Am., Vol. 137, No. 6, June 2015

Laurent *et al.*: Resonances in transversely isotropic cylinder 3333

[18]H. McNiven and Y. Mengi, "Dispersion of waves in transversely isotropic rods," J. Acoust. Soc. Am. **49**, 229–236 (1971).

[19]P. B. Nagy, "Longitudinal guided wave propagation in a transversely isotropic rod immersed in fluid," J. Acoust. Soc. Am. **98**, 454–457 (1995).

[20]M. J. Berliner and R. Solecki, "Wave propagation in fluid-loaded, transversely isotropic cylinders. Part I. Analytical formulation," J. Acoust. Soc. Am. **99**, 1841–1847 (1996); "Wave propagation in fluid-loaded, transversely isotropic cylinders. Part II. Numerical results," *ibid.* **99**, 1848–1853 (1996).

[21]A. J. Niklasson and S. K. Datta, "Scattering by an infinite transversely isotropic cylinder in a transversely isotropic medium," Wave Motion **27**, 169–185 (1998).

[22]F. Ahmad and A. Rahman, "Acoustic scattering by transversely isotropic cylinders," Int. J. Eng. Sci. **38**, 325–335 (2000).

[23]V. Buchwald, "Rayleigh waves in transversely isotropic media," Q. J. Mech. Appl. Math. **14**, 293–317 (1961).

[24]F. Ahmad, "Guided waves in a transversely isotropic cylinder immersed in a fluid," J. Acoust. Soc. Am. **109**, 886–890 (2001).

[25]F. Honarvar and A. Sinclair, "Acoustic wave scattering from transversely isotropic cylinders," J. Acoust. Soc. Am. **100**, 57–63 (1996).

[26]F. Honarvar, E. Enjilela, A. N. Sinclair, and S. A. Mirnezami, "Wave propagation in transversely isotropic cylinders," Int. J. Solids Struct. **44**, 5236–5246 (2007).

[27]F. Honarvar, E. Enjilela, and A. N. Sinclair, "Asymmetric and axisymmetric vibrations of finite transversely isotropic circular cylinders," Acoust. Phys. **55**, 708–714 (2009).

[28]A. N. Norris and A. Shuvalov, "Wave impedance matrices for cylindrically anisotropic radially inhomogeneous elastic solids," Q. J. Mech. Appl. Math. **63**, 401–435 (2010).

[29]A. N. Norris, A. J. Nagy, and F. A. Amirkulova, "Stable methods to solve the impedance matrix for radially inhomogeneous cylindrically anisotropic structures," J. Sound Vib. **332**, 2520–2531 (2013).

[30]R. Chitikireddy, S. K. Datta, A. H. Shah, and H. Bai, "Transient thermoelastic waves in an anisotropic hollow cylinder due to localized heating," Int. J. Solids Struct. **48**, 3063–3074 (2011).

[31]D. A. Hutchins, K. Lundgren, and S. B. Palmer, "A laser study of transient Lamb waves in thin materials," J. Acoust. Soc. Am. **85**, 1441–1448 (1989).

[32]D. Gsell and J. Dual, "Non-destructive evaluation of elastic material properties in anisotropic circular cylindrical structures," Ultrasonics **43**, 123–132 (2004).

[33]C. Prada, O. Balogun, and T. Murray, "Laser based ultrasonic generation and detection of Zero-Group Velocity Lamb waves in thin plates," Appl. Phys. Lett. **87**, 194109 (2005).

[34]C. Prada, D. Clorennec, and D. Royer, "Local vibration of an elastic plate and Zero-Group Velocity Lamb modes," J. Acoust. Soc. Am. **124**, 203–212 (2008).

[35]A. Meitzler, "Backward-wave transmission of stress pulses in elastic cylinders and plates," J. Acoust. Soc. Am. **38**, 835–840 (1965).

[36]D. Clorennec, C. Prada, and D. Royer, "Local and noncontact measurements of bulk acoustic wave velocities in thin isotropic plates and shells using zero group velocity Lamb modes," J. Appl. Phys. **101**, 034908 (2007).

[37]M. Cès, D. Royer, and C. Prada, "Characterization of mechanical properties of a hollow cylinder with zero group velocity Lamb modes," J. Acoust. Soc. Am. **132**, 180–185 (2012).

[38]D. Clorennec, D. Royer, and H. Walaszek, "Nondestructive evaluation of cylindrical parts using laser ultrasonics," Ultrasonics **40**, 783–789 (2002).

[39]D. Mounier, C. Poilâne, H. Khelfa, and P. Picart, "Sub-gigahertz laser resonant ultrasound spectroscopy for the evaluation of elastic properties of micrometric fibers," Ultrasonics **54**, 259–267 (2014).

[40]D. Royer, "Mixed matrix formulation for the analysis of laser-generated acoustic waves by a thermoelastic line source," Ultrasonics **39**, 345–354 (2001).

[41]D. Clorennec, C. Prada, D. Royer, and T. W. Murray, "Laser impulse generation and interferometer detection of Zero Group Velocity Lamb mode resonance," Appl. Phys. Lett. **89**, 024101 (2006).

[42]F. Seco and A. R. Jiménez, "Modelling the generation and propagation of ultrasonic signals in cylindrical waveguides," in *Ultrasonic Waves*, edited by A. A. dos Santos (InTech, Croatia, 2012).

[43]P. Morse and H. Feshbach, *Methods of Theoretical Physics* (McGraw-Hill, New York, 1953).

[44]S. Tokmakova, "Anisotropy of Poisson's ratio in transversely isotropic rocks," AIP Conf. Proc. **1022**, 413–416 (2008).

[45]A. Ballato, "Poisson's ratios of auxetic and other technological materials," IEEE Trans. Ultrason. Ferroelectr. Freq. Control **57**, 7–15 (2010).